Structural Engineering and Mechanics, Vol. 13, No. 1 (2002) 103-116
DOI: http://dx.doi.org/10.12989/sem.2002.13.1.103

Analysis of transversely isotropic hollow toroids using the semi-analytical DQM

W. Jiang† and D. Redekop‡

Department of Mechanical Engineering, University of Ottawa, Ottawa, Ontario, Canada K1N 6N5

Abstract. A solution based on the linear three-dimensional theory of elasticity is developed for vibration and elastostatic problems of hollow toroids. The theory is developed for transversely isotropic toroids of arbitrary thickness, and has the potential to validate some vehicle and aircraft tire models in the linear range. In the semi-analytical method that is adopted Fourier series are written in the circumferential direction, forming a set of two-dimensional problems. These problems are solved using the differential quadrature method. A commercial finite element program is used to determine alternative solutions. For validation both problems of vibration and elastostatics are considered. Finally results are determined for local surface loading problems, and conclusions are drawn.

Key words: toroids; differential quadrature; finite elements.

1. Introduction

Toroidal shells are popular structural forms, finding such applications in engineering as reactor vessels, protective devices for nuclear fuel pellets, bouyancy units, and vehicle and aircraft tires. With the development of new materials there is a demand for new analytical tools to model toroidal shells made of anisotropic, orthotropic, and transversely isotropic materials (Naboulsi *et al.* 2000).

Considerable work has been done on the vibration and elastostatics of thin-walled isotropic toroidal shells (Redekop and Xu 2000, Leung and Kwok 1994, Redekop 1994). Studies have also been conducted of thin-walled laminated toroidal shells with application to vehicle and aircraft tires (Kim *et al.* 1990, Gall *et al.* 1995, Zhang *et al.* 1997, and Darnell *et al.* 1997). In some of these latter studies it has been pointed out that the shells approach a thick-walled status. There is thus a need for an analytical tool to cover thick-walled toroidal shells (hollow toroids), for tire as well as other applications. As well it is desirable to have an independent method available that can serve to validate the finite element method, which is the main tool available in this area at present.

In this study the three-dimensional theory of elasticity is developed to consider the vibration and elastostatics of hollow transversely isotropic toroids with annular cross-section of arbitrary but uniform thickness. Fourier series expansions are written in the circumferential direction leading to a series of two-dimensional problems for the individual harmonics. The problems are solved using the differential quadrature method (DQM). Validation of the method is through the analyis of problems of natural vibration, and elastostatics. Results in each case are found using the DQM and the finite

† Graduate Student
‡ Professor

element method (FEM). Finally results are determined for local surface loading problems, and conclusions are drawn.

2. Toroidal elasticity theory

The hollow toroid has a bend radius R, and an annular cross-section bounded by radii a and b (Fig. 1). A general point in the toroid is defined by a radial coordinate r, and meridional and circumferential angular coordinates ϕ and θ. The toroid is complete and thus extends through 360^o in the circumferential and meridional directions.

A derivation of the governing equations for the linear three-dimensional theory of elasticity in toroidal coordinates has been given for isotropic materials by Redekop (1992). The theory is extended here to cover the case for transversely isotropic materials. The equations of motion in this theory are given by (Redekop 1992, Grigorenko *et al.* 1998)

$$\begin{aligned}
&\frac{\partial \sigma_{rr}}{\partial r} + \frac{1}{r}\frac{\partial \sigma_{r\phi}}{\partial \phi} + \frac{1}{r}(\sigma_{rr} - \sigma_{\phi\phi}) + \frac{1}{\rho}\left[\frac{\partial \sigma_{r\theta}}{\partial \theta} + \cos\phi(\sigma_{rr} - \sigma_{\theta\theta}) - \sin\phi\,\sigma_{r\phi}\right] = \hat{\rho}\frac{\partial^2 u}{\partial t^2} \\
&\frac{\partial \sigma_{r\phi}}{\partial r} + \frac{1}{r}\frac{\partial \sigma_{\phi\phi}}{\partial \phi} + \frac{2}{r}\sigma_{r\phi} + \frac{1}{\rho}\left[\frac{\partial \sigma_{\phi\theta}}{\partial \theta} + \cos\phi\,\sigma_{r\phi} - \sin\phi(\sigma_{\phi\phi} - \sigma_{\theta\theta})\right] = \hat{\rho}\frac{\partial^2 v}{\partial t^2} \\
&\frac{\partial \sigma_{r\theta}}{\partial r} + \frac{1}{r}\frac{\partial \sigma_{\phi\theta}}{\partial \phi} + \frac{1}{r}\sigma_{r\theta} + \frac{1}{\rho}\left[\frac{\partial \sigma_{\theta\theta}}{\partial \theta} + 2\cos\phi\,\sigma_{r\theta} - 2\sin\phi\,\sigma_{\phi\theta}\right] = \hat{\rho}\frac{\partial^2 w}{\partial t^2}
\end{aligned} \tag{1}$$

where $\rho = R + r\cos\phi$, ρ is the mass density and t is the time. The convention for the displacement and stress components present in this theory is given in Fig. 2. The kinematic relations for the case of small displacements are (Redekop 1992)

$$\varepsilon_{rr} = \frac{\partial u}{\partial r}; \qquad \varepsilon_{r\phi} = \frac{1}{2}\left(\frac{1}{r}\frac{\partial u}{\partial \phi} + \frac{\partial v}{\partial r} - \frac{v}{r}\right)$$

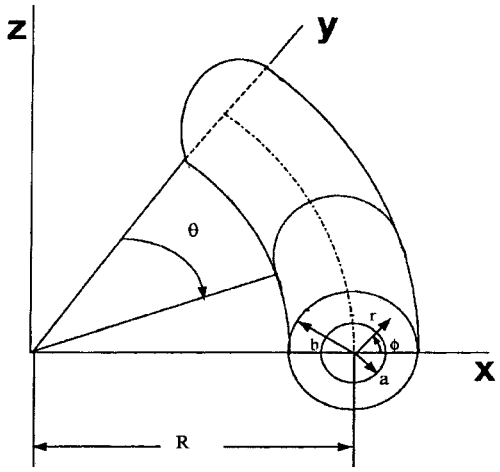

Fig. 1 Geometry and coordinate system

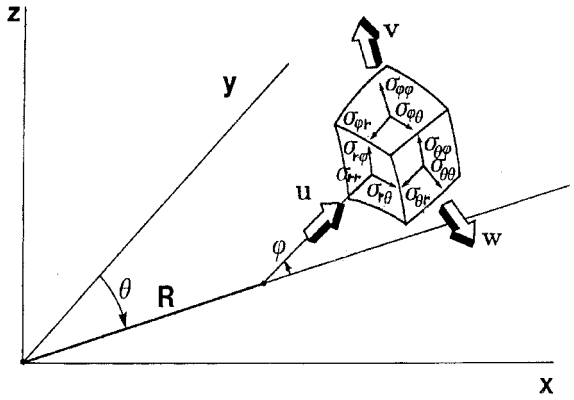

Fig. 2 Displacement and stress components

$$\varepsilon_{\phi\phi} = \frac{u}{r} + \frac{1}{r}\frac{\partial v}{\partial \phi}; \qquad \varepsilon_{r\theta} = \frac{1}{2}\left(\frac{\partial w}{\partial r} + \frac{1}{\rho}\frac{\partial u}{\partial \theta} - \frac{w}{\rho}\cos\phi\right)$$

$$\varepsilon_{\theta\theta} = \frac{1}{\rho}\left(u\cos\phi - v\sin\phi + \frac{\partial w}{\partial \theta}\right); \qquad \varepsilon_{\phi\theta} = \frac{1}{2}\left(\frac{1}{r}\frac{\partial w}{\partial \phi} + \frac{1}{\rho}\frac{\partial v}{\partial \theta} + \frac{w}{\rho}\sin\phi\right) \tag{2}$$

For transversely isotropic materials the constitutive equations are (Grigorenko *et al.* 1998)

$$\begin{pmatrix} \sigma_{rr} \\ \sigma_{\phi\phi} \\ \sigma_{\theta\theta} \\ \sigma_{r\phi} \\ \sigma_{r\theta} \\ \sigma_{\phi\theta} \end{pmatrix} = \begin{bmatrix} d_{11} & d_{12} & d_{13} & 0 & 0 & 0 \\ d_{12} & d_{22} & d_{23} & 0 & 0 & 0 \\ d_{13} & d_{23} & d_{33} & 0 & 0 & 0 \\ 0 & 0 & 0 & d_{44} & 0 & 0 \\ 0 & 0 & 0 & 0 & d_{55} & 0 \\ 0 & 0 & 0 & 0 & 0 & d_{66} \end{bmatrix} \begin{pmatrix} \varepsilon_{rr} \\ \varepsilon_{\phi\phi} \\ \varepsilon_{\theta\theta} \\ \varepsilon_{r\phi} \\ \varepsilon_{r\theta} \\ \varepsilon_{\phi\theta} \end{pmatrix} \tag{3}$$

where the d_{ij} are given by

$$d_{11} = d_{22} = \frac{E' - E(\upsilon')^2}{E(E')^2\Delta}; \quad d_{33} = \frac{1-\upsilon^2}{E^2\Delta}; \quad d_{12} = \frac{\upsilon E' + E(\upsilon')^2}{E(E')^2\Delta}$$

$$d_{13} = \frac{\upsilon'(1+\upsilon)}{EE'\Delta}; \quad d_{23} = \frac{\upsilon'(1+\upsilon)}{EE'\Delta}; \quad d_{44} = 2G; \quad d_{55} = d_{66} = 2G'$$

$$\Delta = \frac{E'(1-\upsilon^2) - 2E(\upsilon')^2(1+\upsilon)}{(EE')^2}; \quad G = \frac{E}{2(1+\upsilon)} \tag{4}$$

The engineering constants υ, υ', E, E', G, G' are respectively the Poisson ratios, Young's moduli, and shear moduli in the in-plane and transverse (θ) directions.

The solution is subject to boundary conditions on the surfaces of the toroid. On the $r = cnst$ surfaces the requirements are

$$\sigma_{rr} = p_i(\theta, \phi); \quad \sigma_{r\theta} = \sigma_{r\phi} = 0 \tag{5}$$

where p_i is a specified pressure with $i = 1$ for the inside surface and $i = 2$ for the outside surface. For some problems symmetry exists about the planes $\phi = 0^o$, $\theta = 0^o$, and $\theta = 90^o$. This symmetry allows consideration of only one-eight of the toroid. In these cases the symmetry conditions

$$v = 0; \quad \sigma_{r\phi} = \sigma_{r\theta} = 0 \tag{6}$$

are satisfied on the plane $\phi = 0^o$, and the symmetry conditions

$$w = 0; \; \sigma_{r\theta} = \sigma_{\phi\theta} = 0$$

are satisfied on the planes $\theta = 0^o$, and $\theta = 90^o$.

For calculation purposes the three-dimensional problem is reduced to a set of two-dimensional ones. In this semi-analytical approach (Kim *et al.* 1990) Fourier series are written in the circumferential direction, and then the various harmonics so defined are dealt with separately. Thus the displacement components and loading are expanded as

$$u = U_o + \Sigma U_n \cos n\theta + \Sigma \overline{U}_n \sin n\theta$$

$$v = V_o + \Sigma V_n \cos n\theta + \Sigma \overline{V}_n \sin n\theta$$
$$w = \Sigma W_n \sin n\theta + \Sigma \overline{W}_n \cos n\theta$$
$$p = P_o + \Sigma P_n \cos n\theta + \Sigma \overline{P}_n \sin n\theta \tag{8}$$

where $n = 1, 2, ..., N$. Governing equations are obtained by combining Eqs. (1-3) with Eq. (8). Two equations are obtained for the unknowns U_o, V_o, three equations for each of the N sets of unknowns U_n, V_n, W_n of the 'even' harmonics, and three equations for each of the N sets of unknowns $\overline{U}_n$, $\overline{V}_n$, $\overline{W}_n$ of the 'odd' harmonics.

The basic equations are used to solve alternatively the problems of vibration and elastostatics for the toroid. In solving the vibration problem the ρ is non-zero, the p_i are zero, and the displacements are taken as harmonics with argument ωt, where ω is the natural frequency. For the elastostatics problem the ρ is taken as zero and the boundary load term p_i represents a static pressure.

3. Differential quadrature method

The DQM approach is used to calculate the solution to the governing equations. This method of numerical analysis was introduced to problems of shell vibration in 1995 (Shu 2000). In the current study the two-dimensional version of the DQM is required with discretization being necessary for the r and ϕ coordinates in each harmonic. As an extended exposition of the DQM approach is given by Shu (2000) only a brief outline is given in the following.

The basis of the DQM is the meshing of the domain and the representation in the domain of the derivatives of a function $f(x)$ by a weighted sum of trial function values, i.e.

$$\left.\frac{d^k f}{dx^k}\right|_{x=x_i} = \sum_{j=1}^{M} A_{ij}^{(k)} f(x_j) \tag{9}$$

Here the $A_{ij}^{(k)}$ are the unknown weighting coefficients of the k-th order derivative at the i-th sampling point of the mesh in the x direction, and M is the number of sampling points in this direction. For the current study sets of trial functions are required for both the radial and meridional directions.

Polynomial trial functions (Shu 2000) are selected for the radial direction, and the variable x represents r. The functions are taken as

$$f(r) = 1, r, r^2, \cdots, r^{M-1} \tag{10}$$

For these functions explicit formulas for the weighting coefficients may be used. For the first order derivative the formulas are

$$A_{ij}^{(1)} = \frac{\pi(r_i)}{(r_i - r_j)\pi(r_j)}; \quad i, j = 1, 2 \ldots, M; \quad i \neq j$$
$$\pi(r_i) = \prod_{j=1}^{M} (r_i - r_j); \quad i \neq j \tag{11}$$

while for the higher order derivatives the formulas are

$$A_{ij}^{(k)} = k\left[A_{ii}^{(k-1)}A_{ij}^{(1)} - \frac{A_{ii}^{(k-1)}}{r_i - r_j}\right]; \quad i, j = 1, 2\ldots, M;\ i \neq j;\ 2 \leq k \leq (M-1)$$

$$A_{ij}^{(k)} = A_{ii}^{(k)} = -\sum_{s=1}^{M} A_{is}^{(k)}; \quad i = 1, 2\ldots, M;\ i \neq s;\ 1 \leq k \leq (M-1) \tag{12}$$

For the sampling points r_i in the radial direction of the mesh the Chebyshev-Gauss-Lobatto spacing (Shu 2000) is used. In this scheme the coordinates r_i are taken as $r_i \equiv x_i = (b–a)y_i$ where the y_i are given by

$$y_1 = 0;\ y_i = \frac{1 - \cos\dfrac{\pi(i-2)}{M-3}}{2};\ 2 < i < (M-1);\ y_M = 1 \tag{13}$$

At each sampling point either the DQM analogue of a governing equation for the domain is represented, or a boundary equation.

Harmonic trial functions (Redekop and Xu 2000) are used in the meridional direction in this problem having cyclic periodicity. Continuity conditions across $\phi = 180^o$, 360^o are then identically satisfied. The trial functions are thus taken as

$$f(\phi) = \cos[2(k-1)\pi\phi]; \quad k = 1, 2, 3,\ldots, \bar{N}/2+1$$
$$f(\phi) = \sin[2(k-\bar{N}/2-1)\pi\phi]; \quad k = \bar{N}/2+2,\ \bar{N}/2+3,\ldots, \bar{N} \tag{14}$$

where $\bar{N}$ is an even number. For equally spaced sampling points in the ϕ direction the weighting coefficients, labelled B_{ij} in the following, may be found explicitly from the inverse of the Vandermonde matrix (Shu 2000).

Use of the quadrature rules (9-14) for the derivatives in the governing equations leads to the transformed DQM domain equations for the nth even harmonic set

$$\begin{aligned}
&(f_1 \Sigma A_{hl}^{(2)} + f_2 \Sigma A_{hl}^{(1)})\, U_{nlj} + (f_3 \Sigma B_{ji}^{(2)} + f_4 \Sigma B_{ji}^{(1)})\, U_{nhi} + f_5 U_{nhj} \\
&+ f_6 \Sigma\Sigma B_{ji}^{(1)} A_{hl}^{(1)} V_{nli} + f_7 \Sigma A_{hl}^{(1)} V_{nlj} + f_8 \Sigma B_{ji}^{(1)} V_{nhi} + f_9 V_{nhj} \\
&+ f_{10} W_{nhj} + f_{11} \Sigma A_{hl}^{(1)} W_{nlj} = \hat{\rho}\frac{\partial^2 U_{nhj}}{\partial t^2}
\end{aligned}$$

$$\begin{aligned}
&f_6 \Sigma\Sigma A_{hl}^{(1)} B_{ji}^{(1)} U_{nli} + f_{12} \Sigma A_{hl}^{(1)} U_{nlj} + f_{13} \Sigma B_{ji}^{(1)} U_{nhi} + f_{14} U_{nhj} \\
&+ (f_{15} \Sigma A_{hl}^{(2)} + f_{16} \Sigma A_{hl}^{(1)})\, V_{nlj} + (f_{17} \Sigma B_{ji}^{(2)} + f_{18} \Sigma B_{ji}^{(1)})\, V_{nhi} \\
&+ f_{19} V_{nhj} + f_{20} \Sigma B_{ji}^{(1)} W_{nhi} + f_{21} W_{nhj} = \hat{\rho}\frac{\partial^2 V_{nhj}}{\partial t^2}
\end{aligned}$$

$$\begin{aligned}
&f_{11} \Sigma A_{hl}^{(1)} U_{nlj} + f_{22} U_{nhj} + f_{23} \Sigma B_{ji}^{(1)} V_{nhi} + f_{21} V_{nhj} + (f_{24} \Sigma A_{hl}^{(2)} \\
&+ f_{25} \Sigma A_{hl}^{(1)}) W_{nlj} + (f_{26} \Sigma B_{ji}^{(1)} + f_{27} \Sigma B_{ji}^{(2)}) W_{nhi} \\
&+ f_{28} W_{nhj} = \hat{\rho}\frac{\partial^2 W_{nhj}}{\partial t^2}
\end{aligned} \tag{15}$$

where the U_{nhj}, V_{nhj}, W_{nhj} are the displacement components at the hj sampling point for the nth harmonic. The functions f_i are given by

$$
\begin{aligned}
&f_1 = a_1;\ f_2 = a_1\,(r^{-1} + \rho^{-1}\cos\phi);\ f_3 = a_2 r^{-2};\ f_4 = -a_2 r^{-1}\rho^{-1}\sin\phi\\
&f_5 = -[n^2 a_3\rho^{-2} + a_9 r^{-2} - (a_4 + a_5) r^{-1}\rho^{-1}\cos\phi + a_6\rho^{-2}\cos^2\phi]\\
&f_6 = (a_2 + a_7) r^{-1};\ f_7 = -(a_2 + a_8)\,\rho^{-1}\sin\phi\\
&f_8 = -r^{-1}[(a_2 + a_9) r^{-1} - a_5\,\rho^{-1}\cos\phi);\ f_9 = -\rho^{-1}\sin\phi\,[(a_4 - a_2) r^{-1} - a_6\rho^{-1}\cos\phi)\\
&f_{10} = n\rho^{-1}[a_4 r^{-1} - (a_3 + a_6)\,\rho^{-1}\cos\phi);\ f_{11} = n\rho^{-1}(a_3 + a_8)\\
&f_{12} = -a_{12}\,\rho^{-1}\sin\phi\,;\ f_{13} = r^{-1}\,[(a_2 + a_9) r^{-1} + (a_2 + a_{13})\rho^{-1}\cos\phi]\\
&f_{14} = -\rho^{-1}\sin\phi\,(a_9 r^{-1} - a_6\rho^{-1}\cos\phi);\ f_{15} = a_2;\ f_{16} = a_2(r^{-1} + \rho^{-1}\cos\phi)\\
&f_{17} = a_9 r^{-2};\ f_{18} = -\,a_9 r^{-1}\rho^{-1}\sin\phi\\
&f_{19} = -[a_{14} n^2\,\rho^{-2} + a_2 r^{-2} + (a_2 + a_{13}) r^{-1}\rho^{-1}\cos\phi + a_6\rho^{-2}\sin^2\phi]\\
&f_{20} = n(a_{13} + a_{14}) r^{-1}\rho^{-1};\ f_{21} = n(a_6 + a_{14})\rho^{-2}\sin\phi\\
&f_{22} = -\rho^{-1}[a_3(\,\rho^{-1}\cos\phi + r^{-1}) + a_{13} r^{-1} + a_6\rho^{-1}\cos^2\phi]\\
&f_{23} = -\,n(a_{13} + a_{14})\,r^{-1}\rho^{-1};\ f_{24} = a_3;\ f_{25} = a_3\,(r^{-1} + \rho^{-1}\cos\phi);\ f_{26} = a_{14} r^{-2}\\
&f_{27} = -a_{14} r^{-1}\rho^{-1}\sin\phi;\ f_{28} = -[(a_6 n^2 + a_{14}\sin^2\phi)\rho^{-2} + a_3\,(\rho^{-1}\cos\phi + r^{-1})\rho^{-1}\cos\phi]
\end{aligned}
\tag{16}
$$

where

$$
\begin{aligned}
&a_1 = d_{11};\ a_2 = d_{44}/2;\ a_3 = d_{55}/2;\ a_4 = d_{13} - d_{23};\ a_5 = d_{12} - d_{23}\\
&a_6 = d_{33};\ a_7 = d_{12};\ a_8 = d_{13};\ a_9 = d_{22};\ a_{10} = d_{12} - d_{33};\ a_{11} = d_{13} - d_{33}\\
&a_{12} = d_{12} - d_{13};\ a_{13} = d_{23};\ a_{14} = d_{66}/2
\end{aligned}
\tag{17}
$$

The assembly of the domain and boundary equations yields a matrix equation of the form

$$
\begin{bmatrix} S_{bb} & S_{bd} \\ S_{db} & S_{dd} \end{bmatrix} \begin{Bmatrix} \Delta_b \\ \Delta_d \end{Bmatrix} - \beta^2 \begin{bmatrix} 0 & 0 \\ 0 & 1 \end{bmatrix} \begin{Bmatrix} \Delta_b \\ \Delta_d \end{Bmatrix} = \begin{Bmatrix} q \\ 0 \end{Bmatrix} \tag{18}
$$

This equation serves as the basis for the solution of the problems of vibration and elastostatics as discussed in the preceding. The vector q contains the load values at the boundary sampling points, and $\beta^2 = (\rho\omega^2\,\overline{r}^{\,2}/E$ is the frequency parameter, where $\overline{r}$ is the mean radius of the cross-section. For the vibration problem the load term q is zero, while for the elastostatic problem the frequency parameter β^2 is zero. The sub-matrices S_{bb} and S_{bd} stem from the boundary conditions, and involve respectively the unknowns of the boundary and domain mesh points. The sub-matrices S_{db} and S_{dd} stem from the governing equations, and similarly involve the the unknowns of the boundary and domain points. The vectors Δ_b and Δ_d contain the displacements of the boundary and domain points respectively. For the vibration problem the latter vector is eliminated using the static condensation technique (Bathe 1996). The matrix Eq. (18) is then reduced into the form

$$
(-S_{db} S_{bb}^{-1} S_{bd} + S_{dd})\ \{\Delta_d\} = \beta^2 \{\Delta_d\} \tag{19}
$$

The smallest eigenvalue is found directly by solving a standard eigenvalue problem.

The theory presented in the preceding was coded in the *MATLAB*^{TM} programs semiom.m and semista.m to cover respectively the vibration and elastostatics problems. Results from these DQM programs are given in the following.

4. Finite element method

The commercial FEM program ADINA (ADINA 2000, Bathe 1996) was used to provide a second solution to the problems considered. Both three-dimensional models consisting of brick elements (ET FEM), and two-dimensional models consisting of shell elements (ST FEM) were used. The brick element in ADINA contains twenty nodes with three displacement degrees of freedom at each node. The shell element is an eight-noded isoparametric element with three displacement and three rotation degrees of freedom at each node.

The models adopted account for symmetry of the geometry and thus represent one eight of a toroid. The three-dimensional model is used to provide a second solution for all cases considered, while the shell theory model is used only for an elastostatics problem involving an isotropic material. Sample meshes for both elasticity and shell theory models are discussed in section 6.

5. Validation

Two problems were solved to obtain partial validation for the DQM solution. The first problem concerns the determination of some natural frequencies of a hollow toroid. The second problem concerns the determination of the stress state in a hollow toroid subjected to a set of band loads.

The geometry of the first validation problem is that of a complete hollow toroid. The polar axisymmetric vibrations of thick toroids were studied earlier by McGill and Lenzen (1967), while thin toroids (toroidal shells) were studied by Balderes and Armenakis (1973). The β^2 values obtained from the program semiom.m for the first five natural frequencies for some thin toroids are compared in Table 1 with those given by Balderes and Armenakas (1973). The sizes given for meshes refer respectively to the radial and meridional directions. In this table and subsequently ET indicates evaluation using the elasticity theory. Also given are frequencies obtained using the ET FEM. The DQM results agree well with the ET FEM results, and there is also good agreement with results given by Balderes and Armenakas (1973). For some thick toroids discussed by McGill and Lenzen (1967) results obtained by the DQM and the ET FEM showed close agreement with each other, but showed major deviation from results given in the 1967 study. The deviations are discussed further by Jiang and Redekop (2001).

Table 1 Thin shell natural frequency parameter β^2

	Shell theory	FEM (ET)		DQM (ET)	
Geometry	Balderes (1973)	Mesh	Value	Mesh	Value
R/r_o =10		2×400	0.0149	6×18	0.0149
h/r_o =0.01	0.0148	2×800	0.0149	8×24	0.0149
		4×800	0.0149	12×36	0.0148
R/r_o =10		2×400	0.0322	6×18	0.0319
h/r_o =0.02	0.0315	2×800	0.0322	8×24	0.0319
		4×800	0.0322	12×36	0.0318
R/r_o =5		2×500	0.0153	6×18	0.0152
h/r_o =0.02	0.0150	2×1000	0.0153	8×24	0.0152
		4×1000	0.0153	12×36	0.0152

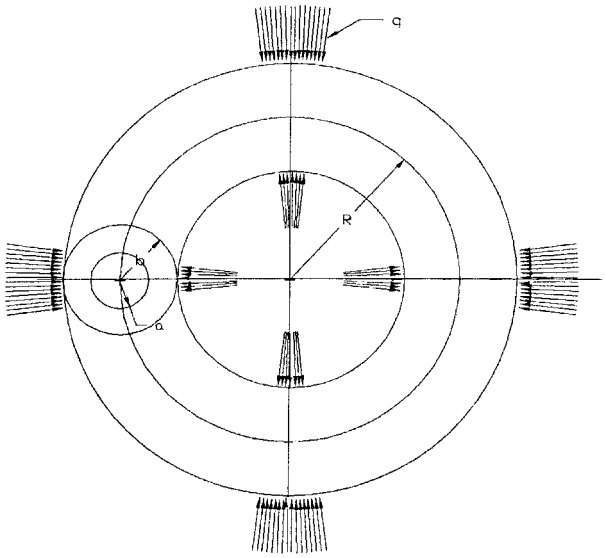

Fig. 3 Band loading of hollow toroid

The geometry for the second validation problem is given in Fig. 3. A hollow steel toroid is subjected to a set of four band loads, each of which extends around the cross-section. The loads are spaced at 90° intervals and have an angular width of 2α. The band loads are on the external surface of the toroid, and produce a unit uniform compression within the bands. Numerical results are found for the case of $a = 100$ mm, $b = 200$ mm, $R = 500$ mm, $\alpha = 8^{o}$. The material properties are $E = 206$ GPa, and $\upsilon = 0.3$. Values for stresses obtained from the program semista.m are compared in Fig. 4 with those given by Zhu and Redekop (1995). The values represented are the meridional stress on the external surface. Also presented are values obtained using the the FEM with three-dimensional

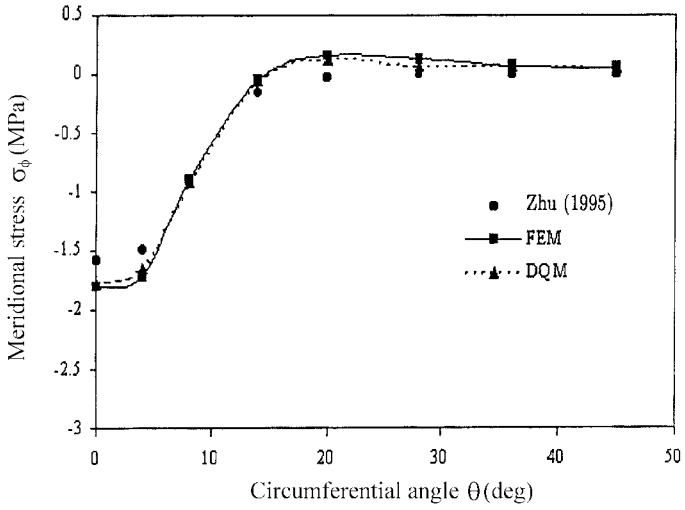

Fig. 4 Meridional stresses for band loading

elements. It is seen that the DQM and FEM results show very close agreement, and that good agreement is also obtained with the results of Zhu and Redekop (1995).

6. Results and discussion

The DQM method and ADINA FEM program are used to obtain natural frequencies, displacements, and stresses for three geometric cases described in Table 2. Symbol $\bar{r}$ in this table indicates the mean radius of the cross-section and h the thickness. The first two cases of the table are thin toroids identical to cases 9 and 10 discussed by Redekop and Zhang (1992). The third case is a thick toroid, outside the range of shell theory. Two materials are considered, steel (isotropic) and M2 (transversely isotropic) (Chandrashekhara and Nanjunda Rao 1997). The properties of the steel material are $\upsilon = 0.3$, $E = 206$ GPa, while for the M2 material the properties are $E = 172.38$ GPa, $E' = 6.90$ GPa, $G = 2.76$ GPa, $G' = 3.45$ GPa, $\upsilon = \upsilon' = 0.25$.

For the elastostatic problem three systems of local loadings are considered. These systems consist respectively of unit normal pressures at the extrados, crown, and intrados, resembling the systems of

Table 2 Shell cases

Case	R (mm)	$\bar{r}$ (mm)	h (mm)
1	600	100	10.6
2	600	100	18.0
3	600	100	30.0

loads described by Redekop and Zhang (1992). The pressures p_1, p_2, and p_3 of Fig. 5 show the three types of systems in the first quadrant. Identical loadings are understood to be applied in the other three quadrants, and thus planes $\theta = 0^o$, $\theta = 90^o$, $\phi = 0^o$ are planes of symmetry.

For the p_1 load the unit normal pressure extends over the range $30^o \leq \theta \leq 60^o$, $0^o \leq \phi \leq 30^o$. For the p_2 load the range is $30^o \leq \theta \leq 60^o$, $75^o \leq \phi \leq 105^o$. This loading represents a 'pinching' of the

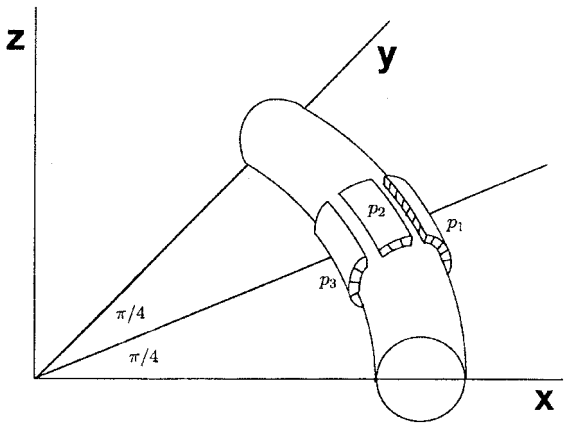

Fig. 5 Local loading cases

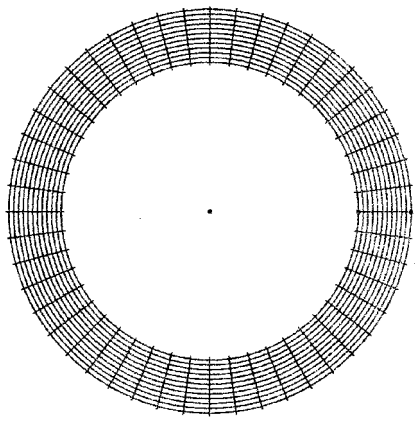

Fig. 6 DQM mesh

toroid since a similar load pad exists on the other side of the $\phi = 0^o$ plane. For the p_3 load the range is $30^o \leq \theta \leq 60^o$, $150^o \leq \theta \leq 180^o$.

Analyses are carried out using the DQM, the ET FEM, and the ST FEM. Typical meshes are given in Figs. 6-8. For the semi-analytical DQM used here the meshing is of a typical cross-section as shown in Fig. 6. The mesh indicated is 48×12, representing respectively points in the meridional and radial directions. Symmetry is accounted for in the FEM analyses, enabling the analysis of one-eigth of the toroid only (Figs. 7-8). The ET FEM mesh of Fig. 7 is of size $2 \times 24 \times 48$, representing respectively points in the radial, meridional, and circumferential directions. The ST FEM mesh of Fig. 8 is of size 24×48, representing respectively points in the meridional and circumferential directions.

The convergence of the solution for the vibration problem is examined in Table 3. The frequency parameter $\rho\omega^2$ for the three geometric cases of Table 2 as found using the DQM and the ET FEM are given for coarse, medium, and fine meshes for each of the two materials. Rapid convergence is observed for both methods. Passing from cases 1 to 3 the frequencies increase (as the wall thickness increases). The frequencies for the steel toroids are higher than those of the M2 material due to the

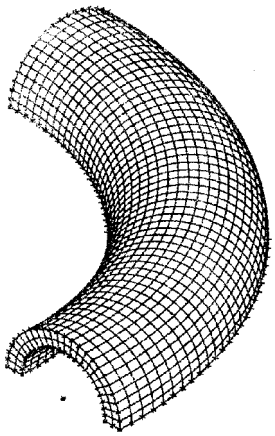

Fig. 7 Elasticity theory FEM mesh

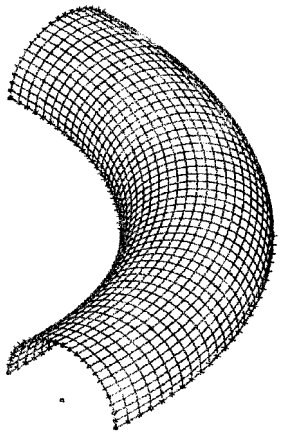

Fig. 8 Shell theory FEM mesh

Table 3 Convergence study - parameter $\hat{\rho}\omega^2$ ($\times 10^9$)

Case	FEM (ET)			DQM (ET)		
	Mesh	Steel	M2	Mesh	Steel	M2
1	$1 \times 12 \times 24$	23.28	2.133	4×24	22.30	2.101
	$1 \times 24 \times 24$	22.99	2.112	6×36	17.23	1.901
	$1 \times 24 \times 48$	22.99	2.112	12×48	17.23	1.900
2	$1 \times 12 \times 24$	32.18	2.844	4×24	32.28	2.924
	$1 \times 24 \times 24$	32.08	2.836	6×36	28.97	2.712
	$1 \times 24 \times 48$	32.08	2.836	12×48	28.94	2.711
3	$1 \times 12 \times 24$	37.91	3.523	4×16	37.88	4.910
	$2 \times 24 \times 24$	37.84	3.509	8×32	36.32	3.454
	$2 \times 24 \times 48$	37.84	3.509	12×48	36.32	3.454

Table 4 Results for unit loadings on steel shell

		DQM (ET)		FEM (ET)		FEM (ST)	
Case	Load at	u (mm)	$\sigma_{\phi\phi}$ (MPa)	u (mm)	$\sigma_{\phi\phi}$ (MPa)	u (mm)	$\sigma_{\phi\phi}$ (MPa)
1		−0.0770	−31.92	−0.0787	−33.86	−0.0749	−25.78
2	Extrados	−0.0320	−16.45	−0.0346	−17.31	−0.0320	−13.16
3		−0.0144	−7.79	−0.0143	−8.21	−0.0126	−5.77
1		−0.0652	−40.18	−0.0692	−40.93	−0.0684	−35.69
2	Crown	−0.0214	−17.17	−0.0227	−18.54	−0.0212	−16.35
3		−0.0070	−7.67	−0.0069	−7.99	−0.0062	−6.95
1		−0.1180	−50.31	−0.1000	−46.35	−0.0974	−35.47
2	Intrados	−0.0373	−20.90	−0.0342	−20.32	−0.0326	−14.80
3		−0.0139	−8.90	−0.0132	−8.87	−0.0121	−5.78

Table 5 Results for unit loadings on M2 shell

		DQM (ET)		FEM (ET)	
Case	Load at	u (mm)	$\sigma_{\phi\phi}$ (MPa)	u (mm)	$\sigma_{\phi\phi}$ (MPa)
1		−0.609	−10.45	−0.553	−10.15
2	Extrados	−0.318	−7.38	−0.292	−7.30
3		−0.160	−4.56	−0.148	−4.54
1		−0.849	−21.98	−0.821	−24.00
2	Crown	−0.300	−10.30	−0.288	−10.98
3		−0.109	−4.88	−0.109	−5.12
1		−1.366	−21.84	−1.219	−20.80
2	Intrados	−0.438	−10.04	−0.405	−9.93
3		−0.156	−4.60	−0.149	−4.68

greater stiffness. The agreement between DQM and FEM is best for the thick shells where the elasticity theory is most applicable. Subsequently in this work the medium mesh was used in the ET DQM analysis, and the fine mesh for the ET FEM analysis.

Results for the three types of loading for the elastostatic problem are given in Tables 4-5 and Figs. 9-12. Table 4 gives results for the isotropic (steel) toroids. The displacements and circumferential stresses for the three geometric cases, subject to the three unit loadings, as determined by the DQM, ET FEM, and ST FEM are given. The displacement values given represent the normal displacement u at the center of the load pad on the outside surface. The stress values given represent the maximum stress under the load pad, on the outside surface. Table 5 gives similar results for the M2 toroids, but determined only by the DQM and the ET FEM.

In Tables 4 and 5 it is seen that passing from geometric cases 1 to 3 the displacements and stresses both decrease due to the increase in wall thickness. Displacements and stresses are generally lowest for loadings at the extrados where the curvature is positive, i.e., of the spherical kind. There is a major increase in the displacement level passing from the steel to the M2 material, but a decrease in the stress level. In general the DQM and FEM elasticity theory results are in close agreement. The FEM shell theory results generally underestimate the elasticity results.

Figs. 9-10 provide information about the variation of displacements and stresses within the toroid

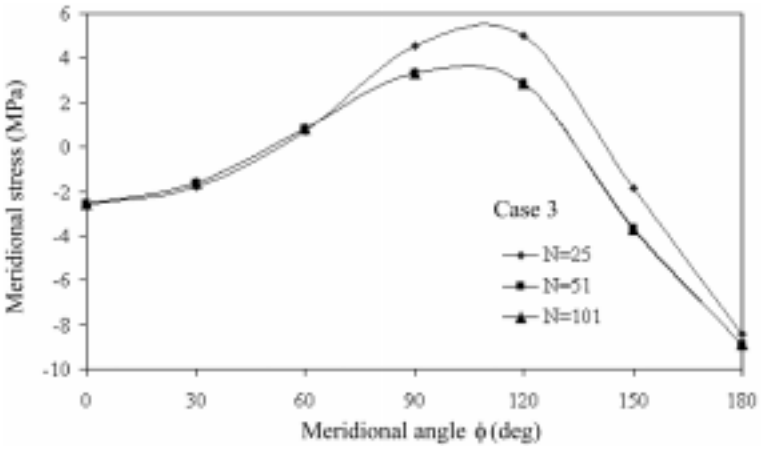

Fig. 9 Convergence of Fourier series

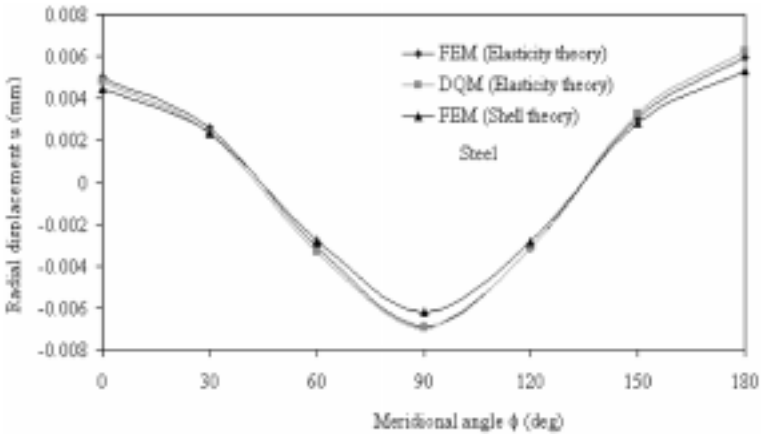

Fig. 10 Radial displacements for p_2 loading

for geometric case 3. Fig. 9 gives the variation of the meridional stress on the outside surface at the $\theta = 45^o$ cross-section for the p_3 loading case as determined by the DQM for a steel toroid. Results are given for a number of different terms in the Fourier series, with convergence indicated at 51 terms.

The variation of the radial displacement u on the outside surface at the $\theta = 45^o$ cross-section for the p_2 loading case as determined by three methods is shown for a steel toroid in Fig. 10. The pinching effect causes an outward displacement at the extrados and intrados, with the latter being greater in magnitute. Simulaneously there is an inward displacement at the crown of similar magnitude.

Fig. 11 shows the variation of the meridional stress on the outside surface at the $\theta = 45^0$ cross-section for the p_2 loading case as determined by three methods for a steel toroid. The shell theory values are seen to underestimate the maximum stress by approximately 10%.

Contour lines are shown in Fig. 12 for the meridional stress on the $\theta = 45^o$ cross-section for the p_3 loading case as determined by the DQM. There is symmetry about the $\phi = 0^o$ plane, i.e., about the 0^o-180^o line on the figure. The higher stress levels clearly are at the intrados, under the loading. The

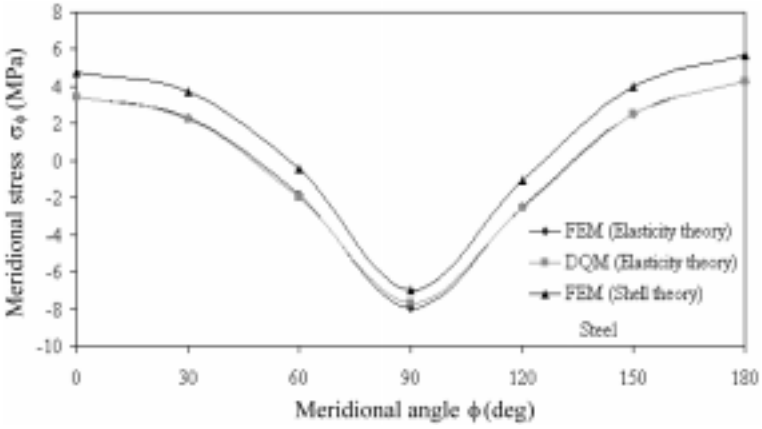

Fig. 11 Meridional stress for p_2 loading

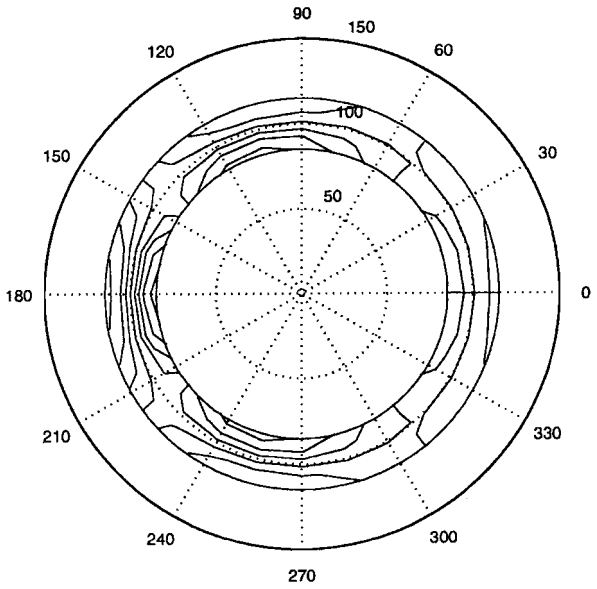

Fig. 12 Contour lines for p_3 loading

variation of stress over the thickness at the intrados clearly deviates from the linear pattern assumed in a shell theory solution.

The previous study by Redekop and Zhang (1992) covered the local loading of steel thin-walled 90^o elbows with 'shear diaphragm' supports at the ends. Cases 9 and 10 of that study are geometrically similar to cases 1 and 2 of the present study, with identical loading patterns. The displacements and stresses cited in Tables 2 and 3 of Redekop and Zhang (1992) are generally higher than the corresponding values given in Table 4 of the current study. This is attributed partially to the more flexible support condition provided by the 'shear diaphragm'. The radial displacement curve for a loading at the extrados shown in Fig. 9 of Redekop and Zhang (1992) is qualitatively similar to the displacement curve given in Fig. 9 of the current study.

7. Conclusions

Results obtained using the theory developed herein agree well with finite element method results both for the vibration and elastostatic problems. The new work provides a valuable efficient tool for the analysis of hollow toroids which can be used to supplement results obtained using the traditional finite element method. To obtain a closer modelling of tire geometries work is currently underway in which the theory is extended to cover hollow toroids of variable thickness.

Acknowledgement

This study was supported in part by a grant from the Natural Sciences and Engineering Research Council of Canada.

References

ADINA, *User's Manual*, **7.4**, ADINA R & D Inc., Waterdown, Mass. (2000).

Balderes, T., and Armenakas, A.E. (1973), "Free vibrations of ring-stiffended toroidal shells," *AIAA J.*, **11**, 1637-1644.

Bathe, K.J. (1996), *Finite Element Procedures*, Prentice Hall, Englewood Cliffs.

Chandrashekhara, K., and Nanjunda Rao, K.S. (1997), "Approximate elasticity solution for a long and thick laminated circular cylindrical shell of revolution," *Int. J. Solids Struct*., **34**, 1327-1341.

Darnell, I., Hulbert, G.M., and Mousseau, C.W. (1997), "An efficient three-dimensional tire model for vehicle dynamics simulations," *Mech. Struct. & Mach*., **25**, 1-19.

Gall, R., Tabaddor, F., Robbins, D., Majors, P., Sheperd, W., and Johnson, S. (1995), "Some notes on the finite element analysis of tires," *Tire Sci. Technol*., **23**, 175-188.

Grigorenko, A. Ya., Dyak, I.I., and Makar, V.M. (1998), "Three-dimensional dynamic elasticity-theory problem for anisotropic bodies," *Int. Appl. Mech.*, **34**(5), 424-430.

Jiang, W., and Redekop, D. (2002), "Polar axisymmetric vibration of a hollow toroid using the differential quadrature method," *J. Sound Vibr*., accepted for publication.

Kim, D.O., Noor, A.K., and Tanner, J.A. (1990), "Modeling and analysis of the space shuttle nose-gear tire with semianalytic finite elements," *NASA TP 2977*, 33 pages.

Leung, A.Y.T., and Kwok, N.T.C. (1994), "Free vibration analysis of a toroidal shell," *Thin-Walled Struct*., **18**, 317-332.

McGill, D.J., and Lenzen, K.H. (1967), "Polar axisymmetric free oscillations of thick hollowed tori," *SIAM Journal*, **15**, 678-692.

Naboulsi, S.K., Palazotto, A.N., and Greer, J.M. (2000), "Static-dynamic analyses of toroidal shells," *J. Aero. Eng*., ASCE, **13**, 110-121.

Redekop, D., and Xu, B. (2000), "Dynamic buckling of toroidal shells subject to impulsive local loading," *Proc. ICPVT-9 Conference*, Sydney, **1**, 685-692.

Redekop, D. (1994), "Natural frequencies of a short curved pipe," *Trans CSME*, **18**, 35-45.

Redekop, D. (1992), "A displacement solution in toroidal elasticity," *Int. J. Pres. Vess. & Piping*, **51**, 189-209.

Redekop, D., and Zhang, F. (1992), "Local loads on a toroidal shell," *J. Strain Analy.*, **27**, 59-66.

Shu, C. (2000), *Differential Quadrature and its Application in Engineering*, Springer, New York.

Zhang, Y., Palmer, T., and Farahani, A. (1997), "A finite element tire model and vibration analysis: a new approach," *Tire Sci. Technol*., **26**, 149-172.

Zhu, Y., and Redekop, D. (1995), "Band loading of a thick-walled toroidal shell," *Int. J. Pres. Vess. & Piping*, **61**, 99-109.